Adsorption (2015) 21:195–204
DOI 10.1007/s10450-015-9662-z

Limitation of adsorptive penetration of cesium into Prussian blue crystallite

Hirotaka Fujita · Risa Miyajima · Akiyoshi Sakoda

Received: 25 September 2014 / Revised: 17 February 2015 / Accepted: 19 February 2015 / Published online: 1 March 2015

Abstract The adsorption of cesium (Cs) onto Prussian blue (PB) with different crystallite sizes is investigated to examine the limitations of the adsorptive penetration of Cs^+ into PB crystallite. The adsorption of Cs^+ onto soluble PB occurs via ion exchange with a charge-compensation cation like K^+, which originally resides in the crystalline lattice. The ratio of the compensation cation sites that are replaced by Cs^+ after adsorption time of 2 weeks significantly increases with decreasing crystallite size, meaning that the adsorption occurs only near the surface of the crystallite during the adsorption time. The depth of Cs^+ penetration after 2 weeks is only within approximately 1–2 nm (or 1–2 units of the crystalline lattice) from the external surface of the crystallite at ambient temperature, regardless of the crystallite size. Hence, the crystallite size is the most important factor governing the adsorption performance.

Keywords Adsorptive penetration · Prussian blue · Cesium

Electronic supplementary material The online version of this article (doi:10.1007/s10450-015-9662-z) contains supplementary material, which is available to authorized users.

H. Fujita (✉) · A. Sakoda
Institute of Industrial Science, University of Tokyo, 4-6-1 Komaba, Meguro-Ku, Tokyo 153-8505, Japan
e-mail: fujiozon@iis.u-tokyo.ac.jp

R. Miyajima
School of Science and Technology, Meiji University, 1-1-1 Higashimita, Tama-Ku, Kawasaki-City, Kanagawa 214-8571, Japan

1 Introduction

Prussian blue (PB) and its analogues (PBA) have been recognized as excellent adsorbents for cesium (Cs) in terms of its high adsorption selectivity (Fujita et al. 2014; Mimura et al. 1997; Thanapon et al. 2010). Since the accident at the Fukushima Daiichi power plant, PB and PBA have attracted increasing attention as a material for use in decontaminating the environment. PB is categorized into two types in terms of its dispersibility and/or its chemical composition: Insoluble and soluble PBs (Buser et al. 1977; Itaya et al. 1986; Keggin and Miles 1936; Louise et al. 2013). Also, various kinds of synthesis methods can provide different sizes and morphologies of crystallites of PB (Hu et al. 2009, 2012a; Louise et al. 2013; Torad et al. 2012; Wu et al. 2006; Zheng et al. 2007). The post-synthesis etching approach also expanded the possibility of morphology control of the PB crystallites (Hu et al. 2012b, c; Torad et al. 2012). On the other hand, the ability of PB to adsorb Cs varies considerably according to its origin such as what synthesis method was used, and under what conditions the PB was prepared (Fujita et al. 2014; Ishizaki et al. 2013; Torad et al. 2012). However, the dominant reason seems to be still unclear. One of the plausible hypotheses is that crystallite size of PB strongly affects the adsorption performance due to penetration limitation of Cs^+ into the crystallite (Fujita et al. 2014; Torad et al. 2012). Our previous study showed that it took quite long time (more than 2 weeks) to attain the adsorption equilibrium onto insoluble PB, even though the crystallite size employed was likely one of the smallest reported in the literature (Fujita et al. 2014). This suggested that the adsorption onto much larger crystallites is expected to be much slower so that it is practically impossible for Cs^+ to penetrate deeply inside the crystallite (Fujita et al. 2014).

Torad et al. suggested that the adsorptive penetration of Cs^+ into the crystallite was limited, demonstrating the localization of adsorbed Cs^+ in the crystallite by elemental mapping (2012). Moritomo et al. demonstrated by ab initio calculations that Cs^+ migration was impossible in the crystallite (2013). Other literature has also pointed to the penetration limitation (Omura and Moritomo 2012; Thanapon et al. 2010). However, the existing literature lacks quantitative evidence. Thus, the objective of this study was to elucidate the limitation of adsorptive penetration of Cs^+ into PB crystallite.

2 Experiment

2.1 Preparation of PB samples

Six kinds of PB with different crystallite sizes were employed. Five kinds of PB (H_3O^+IPB-12, K^+SPB-14, K^+SPB-18, K^+SPB-45, and K^+SPB-800) were synthesized, while commercially available PB (NH_4^+/Na^+SPB-65) was purchased from Kanto Kagaku. The sample names in this study are derived based on (a) whether the sample is soluble (SPB) or insoluble (IPB) (b) what kind of cation was mainly contained, and (c) the crystallite size. Here, we determined whether the sample was IPB or SPB only in terms of the content of an alkali cation or NH_4^+, without considering its dispersibility. That is, we defined the PB sample containing an alkali cation or NH_4^+ as an SPB in this study, while that without an alkali cation or NH_4^+ as an IPB. All the chemicals for synthesis were purchased from Wako. Detailed information regarding the synthesis method is provided in Supplementary Information (Section S1).

2.2 Characterization of PB samples

2.2.1 X-ray diffraction measurement

The powder X-ray diffraction (XRD) pattern of PB was recorded using CuKα radiation by X-ray diffractometer equipped with a diffracted-beam monochrometer (RINT-2000, RIGAKU). Crystallite size was calculated by the Williamson-Hall (WH) method (Georgea et al. 2011). Detailed information regarding the determination of average crystallite size is provided in Supplementary Information (Section S2).

2.2.2 SEM and TEM observations

Scanning electron spectroscopy (SEM) observation of PB samples was performed using JSM-7500 (JEOL). Also, transmission Electron Microscopy (TEM) observation was performed. Detailed information is provided in Supplementary Information (Section S3).

2.3 Adsorption experiment

2.3.1 Cs uptake by prepared PB samples

The PB was added to CsCl aqueous solution at the concentration of 10,000 mg CsCl/L (0.059 mol-Cs/L) or 20,000 mg CsCl/L (0.119 mol-Cs/L), and then a batch adsorption experiment was started with shaking the solution at the rate of 150 rpm at 25 or 60 °C. The ratio of the PB added to the solution was 10 L/g. After 2 weeks, the PB was filtrated and rinsed with 50 cc of water 5 times. After drying at 40 °C for more than 1 day, two methods for inorganic elemental analysis were performed to obtain the Cs/Fe and K/Fe ratios.

2.3.1.1 (A) Analysis of Fe by the phenanthroline method and alkali cations including K^+ and Cs^+ by ion chromatography after low-temperature dry ashing of the PB sample Ten to 30 mg of the PB on a quartz boat was decomposed by a conventional dry-ashing method at low temperature using a tubular furnace. To prevent vaporization of alkali cation, especially Cs, the temperature was slowly increased at a rate of 1 °C/min up to 380 °C, and then maintained for 5 h. In this temperature range, negligible amounts of Cs and K were vaporized (Nonaka et al. 1981, 1985; Tsukada and Nakamura 1999) with complete decomposition of the organic moiety. After cooling to an ambient temperature, 1 cc of 5-mol/L HCl aqueous solution was added to the ash on the quartz boat, followed by heating at 250 °C on a hot plate. As a result, complete drying occurred after complete dissolution of the ash in the HCl solution, and then a red solid was left on the boat. This solid was completely dissolved again to 1 cc of 2 mol/L HCl solution at ambient temperature, followed by dilution to 50 cc with distilled water (Solution (A)). Then, the analyses of Fe and alkali cations were performed separately. Zero to 5 cc of solution (A) was supplied for the phenanthroline method to analyze the content of Fe. The concentration of Fe was measured based on JIS K 0400-57-10. Meanwhile, for the alkali cation analysis, 20 cc of solution (A) was further diluted to 1L with distilled water with addition of zero to 0.5 cc of 30 % H_2O_2, and then subjected to ion chromatography analysis (conductivity detector: CDD-10A VP (Shimazdu); column, IC-C4 (Shimadzu); mobile phase, 1 mM oxalic acid). The H_2O_2 is added to completely remove the small amount of Fe^{2+} dissolved in the prepared solution by oxidizing Fe^{2+} to Fe^{3+}, as the presence of Fe^{2+} hinders accurate determination of the Cs^+ concentration due to the peak overlap in the ion chromatography chart under our experimental

procedure. By this method, more reliable values of Cs/Fe and K/Fe ratios are supposed to be obtained than by XRF. We regarded these values as true Cs/Fe and K/Fe ratios.

2.3.1.2 (B) Analysis of Fe, Cs, and K by X-ray fluorescence (XRF) spectroscopy Inorganic elemental analysis using energy-dispersive X-ray fluorescence spectrometer (JSX-3100R II (JEOL)) was performed without any pretreatment of PB for the calculation of Cs/Fe and K/Fe molar ratios. The correlation between true Cs/Fe and K/Fe ratios and those measured by XRF with the fundamental parameter (FP) method was investigated using 12 PB samples prepared in this study, and sufficiently accurate values for the objective of this study were obtained by XRF using this correlation, as mentioned later. Also, the sample depth to which XRF can analyze is generally several tens of micrometers, although it depends on the composition matrix of the sample. The analysis depth is sufficiently greater than the crystalline size, and thus, we assumed that elemental analysis all over the crystallite is possible using XRF.

2.3.2 Cs uptake during the synthesis of PB

Cs uptake during the synthesis of PB was also investigated. This experiment was based on the synthesis method of K^+SPB-800. In 100 cc of distilled water we dissolved 0.6 g of $K_4[Fe(II)(CN)_6]\cdot 3H_2O$ and 0.96 g of CsCl. In this starting solution, the molar concentrations of Cs^+ and K^+ were the same. Then, 0.3 cc of 10 % NaClO and 1 cc of 35–37 % HCl was added to this solution and kept at 60 °C with stirring at the rate of 130 rpm for 10 h. Thus, the filtrated sample was subject to elemental analysis by XRF to obtain the K/Fe and Cs/Fe ratios.

3 Results and discussion

3.1 Particle structure

Figure 1 shows the XRD patterns. The peaks shown were all ascribed to the PB. The degrees of peak broadening were different, meaning that crystallites of different sizes were successfully prepared. Fig. S1 a and b show an example of the peak fitting and the W–H plot, respectively (see supplementary information). The crystallite size was calculated by the W–H plot for samples except K^+SPB-800. As for K^+SPB-800, the peak width was so narrow that the calculation of crystallite size by the W–H method would yield inaccurate results. Hence, the average crystallite size was roughly estimated by SEM observation. The crystallite sizes are shown in Table S1. As for NH_4^+/Na^+SPB-65, clear observation of an overall image of a primary particle (crystallite) by SEM and estimation of crystallite size by XRD were both possible, as shown in Fig. S2. As a result, both crystallite sizes obtained were similar. The same discussion was also carried out in the literature for much smaller IPB crystallites (Gotoh et al. 2007). TEM images seemed to provide only part of the overall image of the primary particle, as shown in Fig. S2. However, its size also seems to be roughly consistent with XRD results.

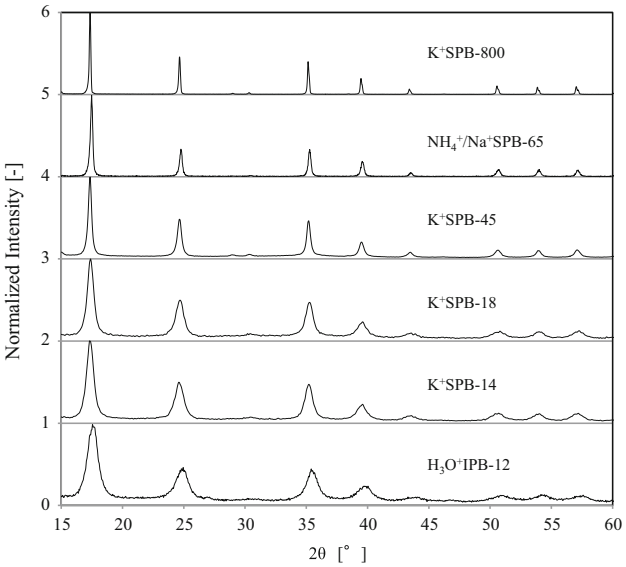

Fig. 1 XRD pattern of each PB prepared

3.2 Adsorption

3.2.1 Dependence of adsorption on crystallite size

Figure 2 shows the correlation between K/Fe and Cs/Fe ratios measured by XRF and their true values. As a result, a linear correlation was obtained, which allowed sufficiently accurate measurement of Cs/Fe and K/Fe ratios by XRF to satisfy the purpose of this study. Hence, the Cs/Fe and K/Fe ratios were mainly analyzed by XRF using this correlation.

Figure 3 shows Cs/Fe and K/Fe ratios of PBs with different crystallite sizes before and after the adsorption of Cs^+. The Cs/Fe ratio increased as a result of adsorption, with (Cs + K)/Fe maintained at almost the same value. This provided quantitative evidence of Cs^+ exchange with K^+ for the K-type PBs (K^+SPB-14, K^+SPB-18, K^+SPB-45, and K^+SPB-800). As for H_3O^+IPB-12, Cs^+ was quantitatively found to be exchanged mainly with H_3O^+ (Fujita et al. 2014; Ishizaki et al. 2013). As for NH_4^+/Na^+SPB-65, the adsorption of Cs^+ was qualitatively confirmed to accompany NH_4^+ and Na^+ release through

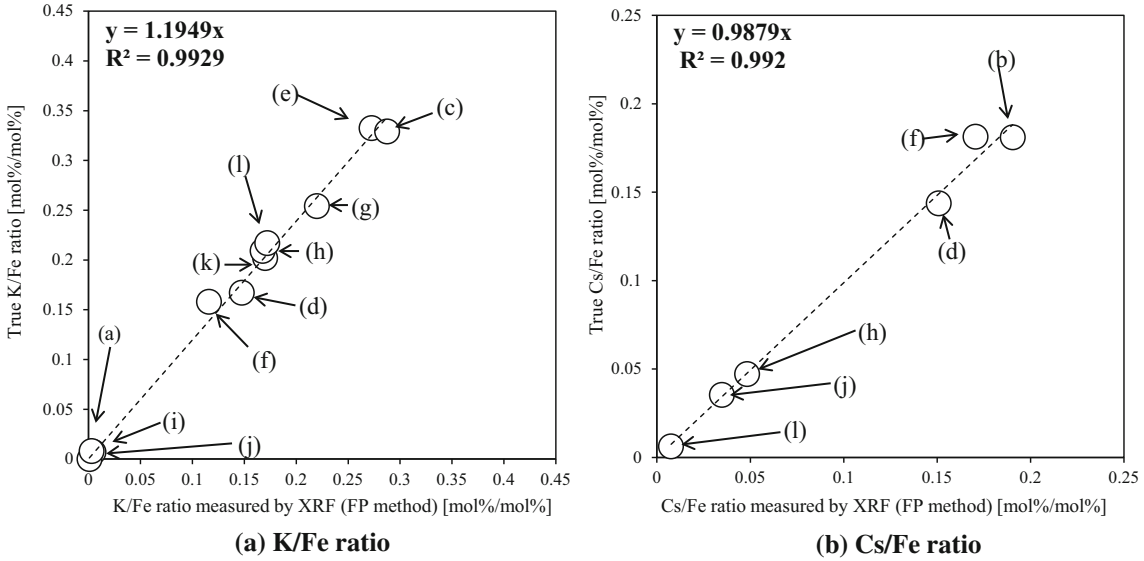

Fig. 2 Correlation between K/Fe and Cs/Fe ratios measured by XRF and their true values. *a* As-synthesized H_3O^+IPB-12, *b* $H3O^+$IPB-12 after Cs^+ adsorption (Cs^+ concentration: 59 mmol/L, temperature: 25 °C), *c* As-synthesized K^+SPB-14, *d* K^+SPB-14 after Cs^+ adsorption (Cs^+ concentration: 59 mmol/L, temperature: 25 °C), *e* As-synthesized K^+SPB-18, *f* K^+SPB-18 after Cs^+ adsorption (Cs^+ concentration: 59 mmol/L, temperature: 25 °C), *g* As-synthesized K^+SPB-45, *h* K^+SPB-45 after Cs^+ adsorption (Cs^+ concentration: 59 mmol/L, temperature: 25 °C), *i* NH_4^+/Na^+SPB-65, *j* NH_4^+/Na^+ SPB-65 after Cs^+ adsorption (Cs^+ concentration: 119 mmol/L, temperature: 25 °C), *k* As-synthesized K^+SPB-800, *l* K^+SPB-800 after Cs^+ adsorption (Cs^+ concentration: 59 mmol/L, temperature: 25 °C)

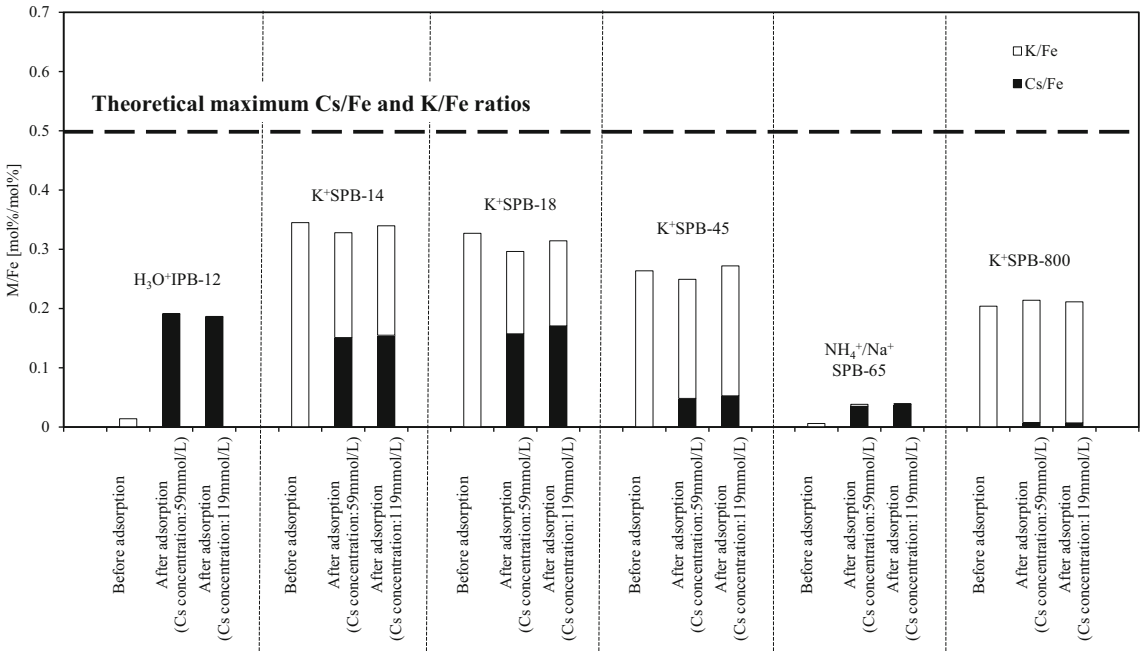

Fig. 3 Cs/Fe and K/Fe ratios before and after the adsorption of Cs (25 °C) (M: K or Cs)

analysis of the supernatant by ion chromatography (data not shown). Figure 3 also demonstrates that the Cs^+ concentration is so high that the adsorption amount after 2 weeks (adsorption time) is almost independent of the Cs^+ concentration under our experimental conditions. It could be roughly said that the ratio of Cs^+ exchange relative to the total amount of K^+ originally residing in the K-type PBs increased with decreasing crystallite size. This seemed to provide direct evidence that the adsorptive penetration of Cs^+ is quite limited.

Here, we discuss the adsorption site of Cs^+, focusing on the fundamental composition, chemical formula and structure of PB. We emphasize in advance that the following discussion is not our original contribution but is used widely for the related fields. However, it seems to be essential for the adsorption mechanism of Cs^+ and quite useful for the whole discussion in this study. $Fe(III)^{3+}$, $[Fe(II)(CN)_6]^{4-}$, and alkali cations like K^+ can be regarded as fundamental parts of PB. Here, we should check the number of $Fe(III)^{3+}$ and $[Fe(II)(CN)_6]^{4-}$ units per unit crystalline lattice "without lattice defects", assuming that the lattice structure is expressed by Fm3 m space group for clarity. Figure 4a shows a well-known simplified lattice structure of PB, which can be reproduced by the structural parameters shown in Fig. 4b-1. In this structure, there are 4 $Fe(III)^{3+}$ cations and 4 $[Fe(II)(CN)_6]^{4-}$ anions per unit lattice, which should give 4 valences of negative charge to the Fe(II)–C–N–Fe(III) framework per unit lattice, and thus 4 monovalent cations are supposed to serve as charge compensation cations. As a result, 8 elements of sub-cubic cells in the unit lattice should be half occupied by the monovalent charge compensation cation, as shown in Fig. 4a. Hence, the K^+ originally residing in the as-synthesized K-type PB can be regarded as the charge compensation cation, and this site is considered an adsorption (ion exchange) site of Cs^+ from our experimental results. As a result, the chemical formula of PB "without lattice defect" is written as $MFe(III)[Fe(II)(CN)_6]$, where M is an alkali cation or NH_4^+. Here, we must mention that PB typically has varying numbers of $[Fe(II)(CN)_6]^{4-}$ vacancies (Buser et al. 1977; Herren et al. 1980; Ishizaki et al. 2013; Louise et al. 2013; Omura and Moritomo 2012). As a result, the vacancy is an important factor determining the amount of charge compensation cations, that is, potential adsorption sites; an increase in the vacancy leads to a decrease in the charge compensation cation sites. Considering this effect, the more general chemical formula of PB is written as $M_{4\alpha-3}Fe(III)[Fe(II)(CN)_6]_\alpha\square_{1-\alpha}$ $(0.75 \leq \alpha \leq 1)$, where $\square$ is the $[Fe(II)(CN)_6]^{4-}$ vacancy (Cafun 2010). Many reports have successfully determined the chemical formula of PB or PBA from the elemental analysis including ICP–MS, CHN, etc., using this simple principle of electrical neutrality (Bleuzen et al. 2008; Cafun et al. 2010; Her et al. 2010; Kareis et al. 2012; Ishizaki et al. 2013; Matsuda et al. 2012;

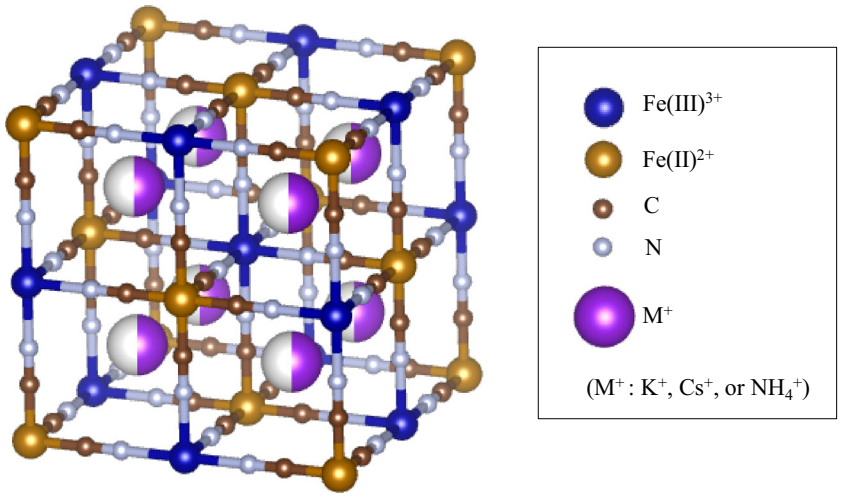

(a) Crystalline lattice of Prussian blue without the $[Fe(CN)_6]^{4-}$ vacancy

(b-1) Structural parameters of Prussian blue without the vacancy, $MFe(III)[Fe(II)(CN)_6]$ (Space group: Fm3m, a (lattice constant) ≒ 10.2Å)

Site	Atom	g	x	y	z
4b	Fe^{3+}	1.0	½	½	½
4a	Fe^{2+}	1.0	0	0	0
24e	C	1.0	x_1	0	0
24e	N	1.0	x_2	0	0
8c	M^+	0.5	¼	¼	¼

(b-2) Structural parameters of Prussian blue with the vacancy, $M_{4\alpha-3}Fe(III)[Fe(II)(CN)_6]_\alpha\square_{1-\alpha}$ (Space group: Fm3m, a ≒ 10.2Å)

Site	Atom	g	x	y	z
4b	Fe^{3+}	1.0	½	½	½
4a	Fe^{2+}	α	0	0	0
24e	C	α	x_3	0	0
24e	N	α	x_4	0	0
8c	M^+	2α-1.5	¼	¼	¼

$(0.75 \leq \alpha \leq 1)$

Fig. 4 Structural parameters, chemical composition and lattice structure of PB

Okubo et al. 2010). As mentioned above, we considered that the charge compensation cation site was the main adsorption site of Cs^+ for "soluble" PB. On the other hand, a completely opposite hypothesis regarding the adsorption site for "insoluble PB" was also proposed by Ishizaki et al. The chemical formula of insoluble PB has been determined as $Fe(III)_4[Fe(II)(CN)_6]_3$ from the elemental analysis and Mössbauer spectroscopy, whose value of α corresponds to 0.75 in the above formula (Buser et al. 1977; Herren et al. 1980; Ito et al. 1968). This means that insoluble PB has no charge compensation cation. Nevertheless, the proton exchange mechanism with Cs^+ is evidently observed for insoluble PB (Fujita et al. 2014; Ishizaki et al. 2013). Ishizaki et al. proposed an adsorption mechanism for IPB with a special focus on coordination and crystallization waters in the lattice defect site to explain the proton exchange mechanism, and implied that the defect site, that is, the $[Fe(II)(CN)_6]^{4-}$ vacancy, is the main adsorption site of Cs^+ (Ishizaki et al. 2013). Hence, there is a possibility that the adsorption site might differ completely between soluble and insoluble PBs. However, at least for the K-type PBs, our experimental results directly and clearly demonstrated that not the $[Fe(II)(CN)_6]^{4-}$ vacancy but rather the charge compensation cation site was the main adsorption site of Cs. Hence, we attempt to further advance the discussion mainly on the adsorption phenomena of K-type PBs, based on this hypothesis regarding the exchange site. From the above generalized chemical formula, the maximum value of the M/Fe ratio is theoretically supposed to be 0.5, in which PB has no $[Fe(II)(CN)_6]^{4-}$ vacancy, as illustrated in Fig. 3. It is reasonable that the measured values of the K/Fe ratio for as-synthesized K-type PB were lower than this value. The difference in the amount of the K^+ site, that is, the potential adsorption site, among K-type PBs seemed to be mainly ascribed to the differences in amounts of the vacancies. Hence, not the absolute value of the Cs/Fe ratio but the ratio of exchangeable sites should be the key issue in discussing the depth of Cs^+ penetration. The penetration depth was roughly estimated with the following assumptions.

- Crystallites are cubic or spherical in shape (See the SEM or TEM image in Fig. S2).
- K^+ sites, that is, possible adsorption sites or vacancies, are located with constant homogeneity throughout the crystallite.
- Through adsorption, Cs^+ occupies a sub-cubic cell of the crystalline lattice beginning at the surface and penetrating toward the core.

As a result, the following equation was given to the relation among the depth of Cs penetration, d, the crystallite size, L, and the ratio of Cs^+-exchangeable K^+ sites to the total original amount of K^+ sites, $X_{exchange}$. This formula can be employed regardless of whether the crystallite shape is cubic or spherical, as shown in Fig. 5.

$$x_{exchange} = 1 - \left(1 - \frac{2d}{L}\right)^3 \quad (1)$$

The calculated results are shown in Table 1a. The estimation was not performed for K^+SPB-800, because the average crystallite size could not be obtained by XRD. The depth of Cs^+ penetration after 2 weeks (adsorption time) was only within approximately 1–2 nm (or 1–2 units of the crystalline lattice) from the external surface of the crystallite at ambient temperature. This result quantitatively showed that the penetration after the adsorption time was limited to just a few layers from the external surface, as for the K-type PBs. The localization of adsorbed Cs^+ was also demonstrated by elemental mapping using TEM-EDX (Torad et al. 2012). Hence, the smaller the crystallite of PB, the more effective the adsorption of Cs, as small crystallites have a greater proportion of surface area.

3.2.2 *Dependence of adsorption on temperature*

Figure 6 shows the dependence of adsorption amount on temperature. The adsorption amount (adsorption time: 2 weeks) increased with increasing temperature, regardless of IPB/SPB status, suggesting that the penetration of Cs^+ was also limited even for the sample with the smallest crystallite size (H_3O-IPB-12). Prior to this experiment, we checked the XRD pattern before and after exposure of H_3O^+IPB-12 to water at 60 °C for 2 weeks, because of the anxiety about degradative change in the structure of PB. As a result, negligible change in crystallite size was confirmed even for the sample with the smallest crystallite size: The crystallite sizes of H_3O^+IPB-12 before and after the exposure were 11.7 ± 3.1 and 11.2 ± 1.0 nm, respectively. Hence, an increase in the Cs/Fe ratio brought by a temperature increase can be interpreted as an increase in the depth of adsorptive penetration. As for the K-type PBs, the penetration depth was significantly increased by the temperature increase, as shown in Table 1b. However, even at 60 °C, the penetration was shallow. It was also confirmed in our previous study that the enhancement of penetration by temperature increase for H_3O^+IPB-12 appeared in a different manner; the adsorption rate -more accurately, the intracrystalline diffusion- was remarkably enhanced by temperature increase (Fujita et al. 2014). This means that the activation energy of intracrystalline diffusion is quite large. Our previous study also showed that the intracrystalline diffusion coefficient was extremely small at less than 3.3×10^{-22} m^2/s (25 °C). Hence, a possible reason for the limitation of the Cs^+ penetration is the extremely

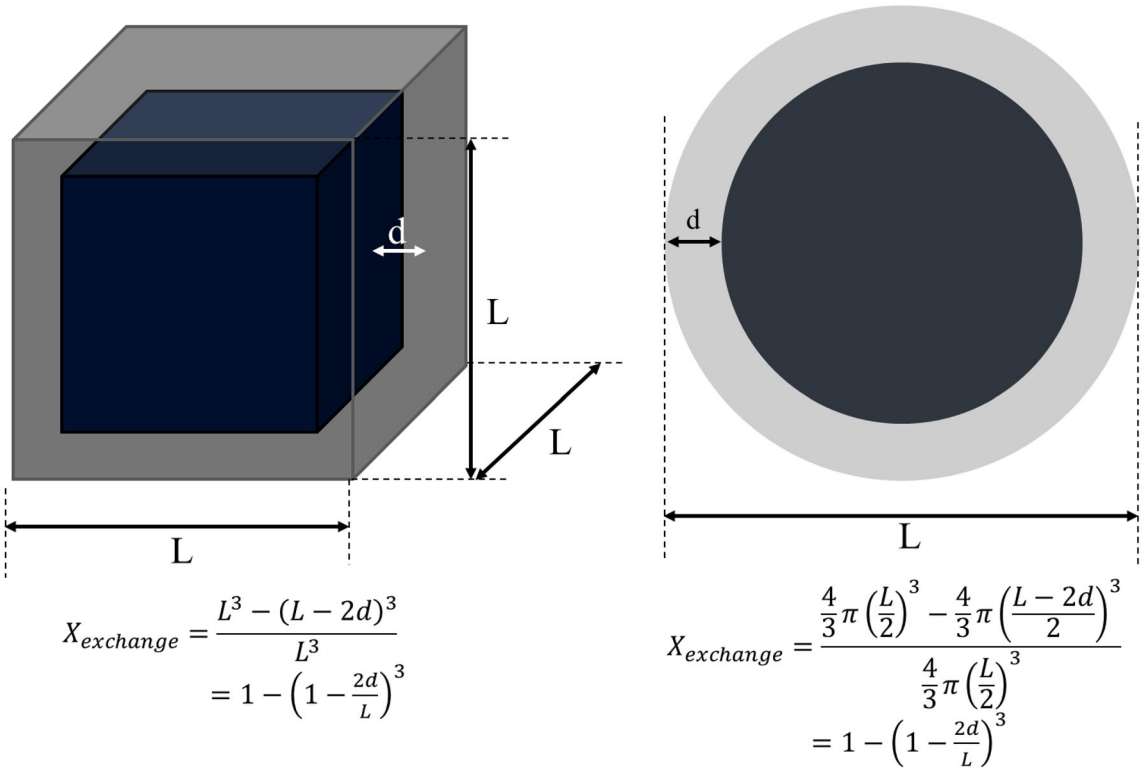

Fig. 5 Relationship among the penetration depth of Cs^+, d, the crystallite size, L, and the ratio of exchangeable K^+ site, $X_{exchange}$

Table 1 Penetration depth of Cs^+

	K^+SPB-14	K^+SPB-18	K^+SPB-45
(a) 25 °C			
L (nm)	14	18	45
d (nm)	1.3	2.0	1.5
$X_{exchangec}$ [−](experiment)	0.46	0.53	0.19
$X_{exchangec}$ [−](calculation)	0.46	0.53	0.19
2d/L[−]	0.19	0.22	0.067
(b) 60 °C			
L (nm)	14	18	45
d (nm)	1.5	2.4	2.1
$X_{exchangec}$ [−](experiment)	0.51	0.60	0.25
$X_{exchangec}$ [−](calculation)	0.51	0.60	0.25
2d/L[−]	0.21	0.27	0.093

large diffusion resistance due to the strong affinity of Cs^+ for the anionic framework: The site-hopping of Cs^+ once strongly bound to the adsorption site of PB might be quite slow or almost impossible, as Thanapon et al. suggested (2010). Also, Moritomo et al. demonstrated that the potential curve of Cs^+ exhibited a barrier at the window of the host framework due to the direct atomic repulsive interaction (2013). Hence, the narrow window could also be a considerable obstacle for the migration of Cs^+.

3.2.3 Uptake of Cs during the synthesis of PB

We investigated the Cs^+ uptake during the synthesis of PB, in which the PB framework was not yet built. To the best of our knowledge, this type of experiment was first attempted for PBAs by the immediate precipitation reaction method by Omura et al. (Omura and Moritomo 2012). They demonstrated the effectiveness of Cs^+ uptake during the synthesis of PBAs (Moritomo et al. 2013; Omura and Moritomo 2012). However, the uptake selectivity for Cs^+ over K^+ during the synthesis of PB (or PBA) has not been clearly elucidated, which is supposed to be the key issue in discussing the intrinsic equilibrium of ion exchange on K-type PB, as mentioned later. Hence, we performed similar experiments using a slow reaction to investigate it. In this synthesis, the main source materials of PB were Cs^+, K^+, $Fe(III)^{3+}$, and $[Fe(CN)_6]^{4-}$, and molar concentrations of Cs^+ and K^+ in the starting synthesis solution were set to be the same, as mentioned in the Experimental section. Also, under the synthesis condition, the formation of soluble PB proceeds quite slowly due to the slow supply of $Fe(III)^{3+}$ such that a quite large crystallite in the range of several hundred nanometers to several micrometers can be constructed (Wu et al. 2006), and hence the uptake of alkali cation could occur thermodynamically rather than kinetically during the synthesis. As a result, the Cs-type PB

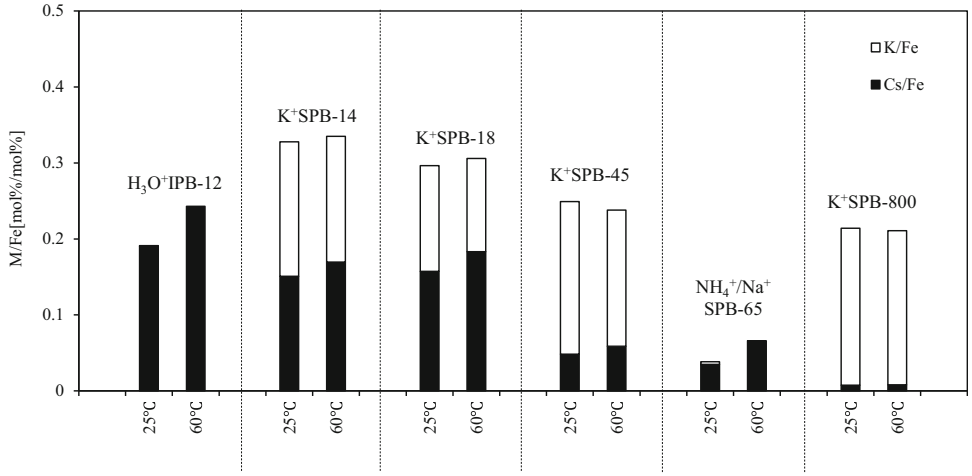

Fig. 6 Effect of temperature on the saturated adsorption amount of Cs^+ (Cs^+ concentration: 59 mmol/L) (M: K^+ or Cs^+)

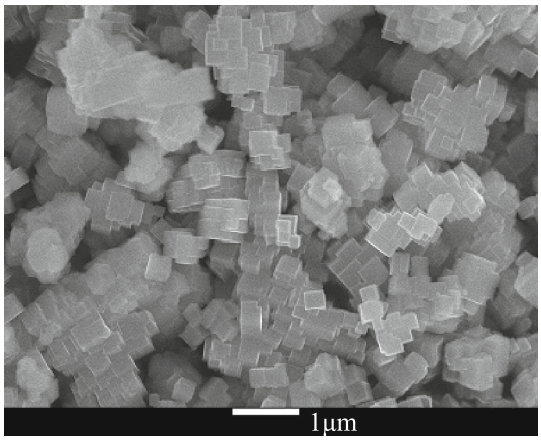

(a) SEM image of the Cs-type PB

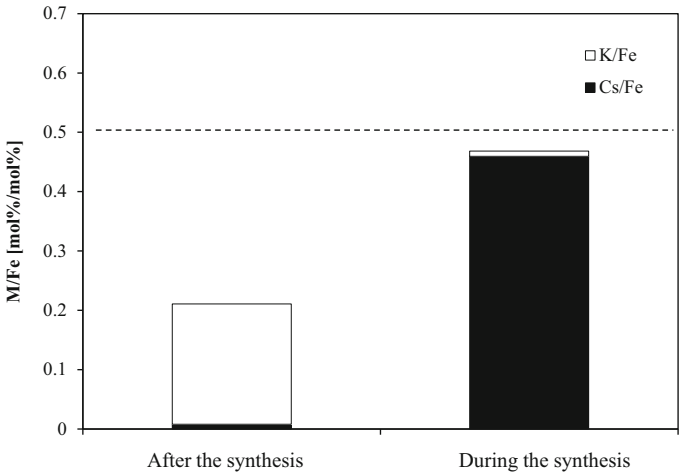

(b) Cs/Fe and K/Fe ratios after the uptake of Cs^+ (Experimental conditions of Cs^+ uptake by PB after the synthesis: K^+SPB-800 (adsorbent), 59mmol/L (Cs^+ concentration), 60 ℃(temperature))

Fig. 7 Comparison of Cs^+ uptake between during and after the synthesis

could be synthesized with little K^+ contained, meaning that the uptake selectivity of Cs^+ was extremely high even during the synthesis, as shown in Fig. 7b. This also suggested that the formation of Cs-type PB (or the lattice containing Cs^+) was entirely predominant over that of K-type PB (or the lattice containing K^+). In addition, the result demonstrated the possibility of deep and highly selective incorporation of Cs^+ into a large PB crystallite within 10 h (synthesis period), even in the presence of high concentration of K^+ in the solution, which was impossible after the synthesis; that is, after the construction of the crystalline lattice containing K^+. The crystallite size of the Cs-type PB was confirmed to be approximately 200 nm from the SEM observation, as shown in Fig. 7a. Except for the uptake selectivity, essentially similar results have already been reported for PBAs (Moritomo et al. 2013; Omura and Moritomo 2012). The formation of Cs-type and K-type PBs is described in the following chemical equations.

$$(4\alpha - 3)Cs^+ + \alpha[Fe(II)(CN)_6]^{4-} + Fe(III)^{3+} \rightarrow Cs_{4\alpha-3}Fe(III)[Fe(II)(CN)_6]_\alpha \quad (2)$$
$$\Delta G_{CsPB\ formation}$$

$$(4\beta - 3)K^+ + \beta[Fe(II)(CN)_6]^{4-} + Fe(III)^{3+} \rightarrow K_{4\beta-3}Fe(III)[Fe(II)(CN)_6]_\beta \quad (3)$$
$$\Delta G_{KPB\ formation}$$

where $\Delta G_{CsPB\ formation}$ and $\Delta G_{KPB\ formation}$ are the Gibbs free energies of formation of $Cs_{4\alpha\text{-}3}Fe(III)[Fe(II)(CN)_6]_\alpha$ and $K_{4\beta\text{-}3}Fe(III)[Fe(II)(CN)_6]_\beta$, respectively. Both free energies should be highly negative, given the stability of PB in water. Nevertheless, the entire predominance of

Cs-type PB formation can be interpreted as a large difference between $\Delta G_{\text{CsPB formation}}$ and $\Delta G_{\text{KPB formation}}$. Here, we assume that the values of α and β are the same. Under this rough assumption, the Gibbs free energy of ion exchange, $\Delta G_{\text{ion exchange}}$, can be described as follows.

$$\begin{aligned}&(4\alpha-3)\mathrm{Cs}^{+}+\mathrm{K}_{4\alpha-3}\mathrm{Fe}\left[\mathrm{Fe}(\mathrm{CN})_6\right]_{\alpha}\\&\quad\rightarrow(4\alpha-3)\mathrm{K}^{+}+\mathrm{Cs}_{4\alpha-3}\mathrm{Fe}\left[\mathrm{Fe}(\mathrm{CN})_6\right]_{\alpha}\\&\Delta G_{\text{ion exchange}}=\Delta G_{\text{CsPB formation}}-\Delta G_{\text{KPB formation}}\end{aligned}\quad(4)$$

In conclusion, the entire predominance of Cs-type PB formation during the synthesis should lead to the excellent adsorption ability of solid PB under adsorption equilibrium; the Gibbs free energy of ion exchange is supposed to be highly negative even in inner layers of the crystallite. However, the ion exchange could be entirely under kinetic control for a relatively large crystallite of PB due to the poor site-hopping ability of Cs^+, as shown in Fig. 7b.

4 Conclusion

The adsorption of Cs^+ onto soluble PB occurs via ion exchange with a charge-compensation cation like K^+, which originally resides in the crystalline lattice. Hence, there is a possibility that the mechanism of Cs^+ adsorption onto soluble PB is completely different from that onto insoluble PB that is considered to have no charge-compensation cation. Nevertheless, quite slow diffusion of Cs^+ in the crystallite is common to both PBs. All the compensation cation sites are considered the potential adsorption sites for soluble PB. However, the ion exchange could be entirely under kinetic control for a relatively large crystallite of soluble PB due to poor site-hopping ability of Cs^+. The considerable dependence of Cs^+ adsorption on temperature indicates the diffusive process with high activation energy. The depth of Cs^+ penetration into K-type PB after 2 weeks (adsorption time) is only within approximately 1–2 nm (or 1–2 units of the crystalline lattice) from the external surface of the crystallite at ambient temperature, regardless of the crystallite size. Hence, the crystallite size is the most important factor governing the adsorption performance.

References

Bleuzen, A., Cafun, J.D., Bachschmidt, A., Verdaguer, M., Münsch, P., Baudelet, F., Itié, J.T.: Co Fe Prussian blue analogues under variable pressure. evidence of departure from cubic symmetry: X-ray diffraction and absorption study. J. Phys. Chem. C **112**(45), 17709–17715 (2008)

Buser, H.J., Schwarzenbach, D., Petter, W., Ludi, A.: The crystal structure of Prussian blue: $Fe_4[Fe(CN)_6]_3.xH_2O$. Inorg. Chem. **16**(11), 2704–2710 (1977)

Cafun, J.D., Champion, G., Arrio, M.A., Moulin, C.C., Bleuzen, A.: Photomagnetic CoFe Prussian blue analogues: role of the cyanide ions as active electron transfer bridges modulated by cyanide-alkali metal ion interactions. J. Am. Chem. Soc. **132**(33), 11552–11559 (2010)

Fujita, H., Sasano, H., Miyajima, R., Sakoda, A.: Adsorption equilibrium and kinetics of cesium onto insoluble Prussian blue synthesized by an immediate precipitation reaction between Fe^{3+} and $[Fe(CN)_6]_4^-$. Adsorption **20**, 905–915 (2014)

Gotoh, A., Uchida, H., Ishizaki, M., Satoh, T., Kaga, S., Okamoto, S., Ohta, M., Sakamoto, M., Kawamoto, T., Tanaka, H., Tokumoto, H., Hara, S., Shiozaki, H., Yamada, M., Miyake, M., Kurihara, M.: Simple synthesis of three primary colour nanoparticle inks of Prussian blue and its analogues. Nanotechnology **18**, 345609–345615 (2007)

Her, J.H., Stephens, P.W., Kareis, C.M., Moore, J.G., Min, K.S., Park, J.W., Bali, G., Kennon, B.S., Miller, J.S.: Anomalous non-Prussian blue structures and magnetic ordering of $K_2Mn(II)[Mn(II)(CN)_6]$ and $Rb_2Mn(II)[Mn(II)(CN)_6]$. Inorg. Chem. 15 **49**(4), 1524–1534 (2010)

Herren, F., Fischer, P., Ludi, A., Haelg, W.: Neutron diffraction study of Prussian Blue, $Fe_4[Fe(CN)_6]_3.xH_2O$. Location of water molecules and long-range magnetic order. Inorg. Chem. **19**(4), 956–959 (1980)

Hu, M., Jiang, J.S., Ji, R.P., Zeng, Y.: Prussian Blue mesocrystals prepared by a facile hydrothermal method. Cryst. Eng. Comm **11**, 2257–2259 (2009)

Hu, M., Torad, N.L., Chiang, Y.D., Wu, K.C., Yamauchi, Y.: Size- and shape-controlled synthesis of Prussian blue nanoparticles by a polyvinylpyrrolidone-assisted crystallization process. Cryst. Eng. Commun. **14**, 3387–3396 (2012a)

Hu, M., Furukawa, S., Ohtani, R., Sukegawa, H., Nemoto, Y., Reboul, J., Kitagawa, S., Yamauchi, Y.: Synthesis of Prussian blue nanoparticles with a hollow interior by controlled chemical etching. Angew. Chem. Int. Ed. **51**, 984–988 (2012b)

Hu, M., Torad, N.L., Yamauchi, Y.: Preparation of various Prussian blue analogue hollow nanocubes with single crystalline shells. Eur. J. Inorg. Chem. **2012**, 4795–4799 (2012c)

Ishizaki, M., Akiba, S., Ohtani, A., Hoshi, Y., Ono, K., Matsuba, M., Togashi, T., Kananizuka, K., Skamoto, M., Takahashi, A., Kawamoto, T., Tanaka, H., Watanabe, M., Arisaka, M., Nankawad, T., Kurihara, M.: Proton-exchange mechanism of specific Cs^+ adsorption via lattice defect sites of Prussian blue filled with coordination and crystallization water molecules. Dalton Trans. **42**, 16049–16055 (2013)

Itaya, K., Uchida, I., Vernon, D.N.: Electrochemistry of polynuclear transition metal cyanides: Prussian blue and its analogues. Acc. Chem. Res. **19**(6), 162–168 (1986)

Ito, A., Suenaga, M., Ono, K.: Mössbauer study of soluble Prussian blue, insoluble Prussian blue, and Turnbull's blue. J. Chem. Phys. **48**, 3597–3599 (1968)

Kareis, C.M., Lapidus, S.H., Her, J.H., Stephens, P.W., Miller, J.S.: Non-Prussian blue structures and magnetic ordering of Na_2-MnII[MnII$(CN)_6$] and Na_2MnII[MnII$(CN)_6]\cdot 2H_2O$. J. Am. Chem. Soc. **134**(4), 2246–2254 (2012)

Keggin, J.F., Miles, F.D.: Structures and formula of the Prussian blues and related compounds. Nature **137**, 577–578 (1936)

Louise, S., Fernande, G., Gary, J.L., Pauline, N., Pierre, B., David, S.: Relationship between the synthesis of Prussian blue pigments, their color, physical properties, and their behavior in paint layers. J. Phys. Chem. C **117**(19), 9693–9712 (2013)

Matsuda, T., Kim, J., Moritomo, Y.: Control of the alkali cation alignment in Prussian blue framework. Dalton Trans. **41**, 7620–7623 (2012)

Mimura, H., Lehto, J., Harjula, R.: Ion exchange of cesium on Potassium nickel hexacyanoferrate(II). J. Nucl. Sci. Technol. **34**(5), 484–489 (1997)

Moritomo Y., Tanaka H.: Alkali cation potential and functionality in the nanoporous Prussian blue analogues. Adv. Condens. Matter Phys. **539620** (2013)

Nonaka, N., Higuchi, H., Hamaguchi, H., Tomura, K.: Losses of the elements during ashing of plant materials. Bunseki Kagaku **30**, 599–604 (1981). (in Japanese, with English abstract)

Nonaka, N., Higuchi, H., Hamaguchi, H., Tomura, K.: Losses of elements during dry ashing of standard reference materials (orchard leaves); relationship between ashing temperature, ashing time, and elemental loss. Bunseki Kagaku **34**(6), 360–364 (1985). (in Japanese, with English abstract)

Okubo, M., Asakura, D., Mizuno, Y., Kim, J.D., Mizokawa, T., Kudo, T., Honma, I.: Switching redox-active sites by valence tautomerism in Prussian blue analogues $A_xMn_y[Fe(CN)_6]\cdot nH_2O$ (A: K, Rb): robust frameworks for reversible Li storage. J. Phys. Chem. Lett. **1**(14), 2063–2071 (2010)

Omura, A., Moritomo, Y.: Cs^+ trapping in size-controlled nanospaces of hexacyanoferrates. Appl. Phys. Express **5**, 057101 (2012)

Thanapon, S., Vichaya, S., Robert, J.W., Rafal, M.G., Glen, E.F., Shane, A., Charles, T., Wassana, Y.: Selective capture of cesium and thallium from natural waters and simulated wastes, with copper ferrocyanide functionalized mesoporous silica. J. Hazard. Mater. **182**(1–3), 225–231 (2010)

Torad, N.L., Hu, M., Imura, M., Naito, M., Yamauchi, Y.: Large Cs adsorption capability of nanostructured Prussian blue particles with high accessible surface areas. J. Mater. Chem. **22**, 18261–18267 (2012)

Tsukada, H., Nakamura, Y.: Transfer of ^{137}Cs and stable Cs from soil to potato in agricultural fields. Sci. Total Environ. **228**, 111–120 (1999)

Wu, X., Cao, M., Hu, C., He, X.: Sonochemical synthesis of Prussian blue nanocubes from a single-source precursor. Cryst. Growth Des. **6**(1), 26–28 (2006)

Zheng, X.J., Kuang, Q., Xu, T., Jiang, Z.Y., Zhang, S.H., Xie, Z.X., Huang, R.B., Zheng, L.X.: Growth of Prussian blue microcubes under a hydrothermal condition: possible nonclassical crystallization by a mesoscale self-assembly. J. Phys. Chem. C **111**, 4499–4502 (2007)